LETTER

doi:10.1038/nature12154

A key role for mitochondrial gatekeeper pyruvate dehydrogenase in oncogene-induced senescence

Joanna Kaplon[1], Liang Zheng[2]*, Katrin Meissl[1]*, Barbara Chaneton[2], Vitaly A. Selivanov[3,4], Gillian Mackay[2], Sjoerd H. van der Burg[5], Elizabeth M. E. Verdegaal[5], Marta Cascante[3,4], Tomer Shlomi[6,7], Eyal Gottlieb[2] & Daniel S. Peeper[1]

In response to tenacious stress signals, such as the unscheduled activation of oncogenes, cells can mobilize tumour suppressor networks to avert the hazard of malignant transformation. A large body of evidence indicates that oncogene-induced senescence (OIS) acts as such a break, withdrawing cells from the proliferative pool almost irreversibly, thus crafting a vital pathophysiological mechanism that protects against cancer[1–5]. Despite the widespread contribution of OIS to the cessation of tumorigenic expansion in animal models and humans, we have only just begun to define the underlying mechanism and identify key players[6]. Although deregulation of metabolism is intimately linked to the proliferative capacity of cells[7–10], and senescent cells are thought to remain metabolically active[11], little has been investigated in detail about the role of cellular metabolism in OIS. Here we show, by metabolic profiling and functional perturbations, that the mitochondrial gatekeeper pyruvate dehydrogenase (PDH) is a crucial mediator of senescence induced by $BRAF^{V600E}$, an oncogene commonly mutated in melanoma and other cancers. $BRAF^{V600E}$-induced senescence was accompanied by simultaneous suppression of the PDH-inhibitory enzyme pyruvate dehydrogenase kinase 1 (PDK1) and induction of the PDH-activating enzyme pyruvate dehydrogenase phosphatase 2 (PDP2). The resulting combined activation of PDH enhanced the use of pyruvate in the tricarboxylic acid cycle, causing increased respiration and redox stress. Abrogation of OIS, a rate-limiting step towards oncogenic transformation, coincided with reversion of these processes. Further supporting a crucial role of PDH in OIS, enforced normalization of either PDK1 or PDP2 expression levels inhibited PDH and abrogated OIS, thereby licensing $BRAF^{V600E}$-driven melanoma development. Finally, depletion of PDK1 eradicated melanoma subpopulations resistant to targeted BRAF inhibition, and caused regression of established melanomas. These results reveal a mechanistic relationship between OIS and a key metabolic signalling axis, which may be exploited therapeutically.

We compared the metabolism of human diploid fibroblasts (HDFs) undergoing OIS to that of cycling cells. To evoke OIS, we used oncogenic $BRAF^{V600E}$, a common oncogene and strong inducer of OIS both *in vitro* and *in vivo*[12–16]. We first analysed the oxygen consumption rate (OCR). Compared to cycling cells, 'OIS cells' showed a significant increase in the OCR, indicating increased mitochondrial oxidative metabolism (Fig. 1a). This was further supported by exchange rate (uptake or secretion) measurements of key metabolites: OIS cells secreted less than half the amount of pyruvate compared with cycling cells, and this was balanced by neither a significant change in glucose consumption nor an increase in lactate or alanine secretion (Fig. 1b, c and Supplementary Fig. 2a, b). Whereas glutamate secretion was increased in OIS cells (Fig. 1d), glutamine consumption was decreased (Supplementary Fig. 2c). In agreement with increased tricarboxylic acid (TCA) cycle activity in OIS cells, stable isotope labelling with a uniformly labelled [U-$^{13}C_6$]glucose tracer showed faster accumulation of glucose-derived 2-carbon-labelled metabolic isotopomers of the TCA cycle (citrate, α-ketoglutarate and malate) as well as TCA cycle-derived 2-carbon-labelled glutamate (Supplementary Fig. 2d). Together, these results indicate that OIS is accompanied by increased pyruvate oxidation, which was corroborated by a simultaneous rise in redox stress, as measured by increased reactive oxygen species (ROS) production, a decrease in the reduced/oxidized glutathione (GSH/GSSG) ratio, and induction of several ROS-responsive genes (Supplementary Fig. 3a–i).

The gatekeeping enzyme linking glycolysis to the TCA cycle is PDH[17,18], which is regulated by reversible phosphorylation[19–22]: phosphorylation by PDK enzymes (PDK1–4) inhibits its action and halts pyruvate use in the TCA cycle, whereas dephosphorylation by PDP1 and PDP2 stimulates PDH activity. Our metabolic profiles predicted PDH to be activated in OIS. Furthermore, if increased PDH activity has a causal role in mediating OIS, we expected this to be reversed after

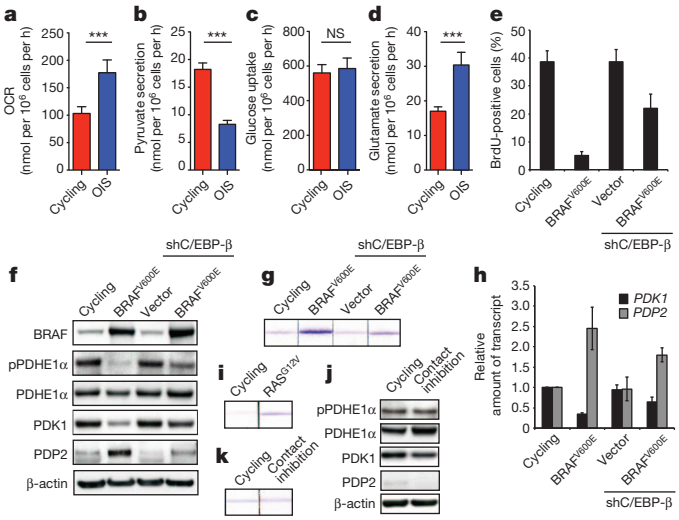

Figure 1 | The PDK1–PDP2–PDH axis is deregulated in OIS. a–d, Analysis of the OCR (**a**), pyruvate secretion (**b**), glucose uptake (**c**) and glutamate secretion (**d**) in cycling and OIS HDFs (after expression of $BRAF^{V600E}$); $n = 6$. **e–h**, Cycling cells and cells undergoing OIS or abrogating OIS (using shC/EBP-β) were analysed for BrdU incorporation (**e**), by immunoblotting (**f**), for PDH activity (**g**) and for regulation of *PDK1* and *PDP2* transcripts, as determined by quantitative reverse transcriptase PCR (qRT–PCR) (**h**); $n = 3$. pPDHE1α denotes phosphorylated PDHE1α. **i**, PDH activity of HDFs undergoing RAS^{G12V}-induced senescence. **j**, **k**, Immunoblotting analysis (**j**) or PDH activity (**k**) of cycling and quiescent HDFs. All data represent mean ± s.d. $^{***}P < 0.001$.

[1]Division of Molecular Oncology, The Netherlands Cancer Institute, Plesmanlaan 121, 1066 CX Amsterdam, The Netherlands. [2]Cancer Research UK, Beatson Institute for Cancer Research, Switchback Road, Glasgow G61 1BD, UK. [3]Department of Biochemistry and Molecular Biology and IBUB, Faculty of Biology, Universitat de Barcelona, Av Diagonal 643, 08028 Barcelona, Spain. [4]Institut d'Investigacions Biomèdiques August Pi i Sunyer (IDIBAPS), Rosselló 149-153, 08036 Barcelona, Spain. [5]Experimental Cancer Immunology and Therapy, Department of Clinical Oncology, Leiden University Medical Center, Albinusdreef 2, 2333 ZA Leiden, The Netherlands. [6]Computer Science Department, Technion, Israel Institute of Technology, Haifa 32000, Israel. [7]Lewis-Sigler Institute for Integrative Genomics, Princeton University, Princeton, New Jersey 08544, USA.

*These authors contributed equally to this work.

OIS escape (by C/EBP-β depletion[13] or SV40 small-t-antigen expression; Fig. 1e and Supplementary Fig. 4a). Indeed, PDH phosphorylation (on Ser 293, one of three phosphorylation sites inactivating PDH) was strongly reduced in OIS cells, but this was restored after senescence abrogation (Fig. 1f and Supplementary Fig. 4b). These changes in PDH phosphorylation translated into corresponding alterations in its activity (Fig. 1g).

Notably, in OIS cells, the two key PDH-modifying enzymes were regulated in opposite directions: whereas PDK1 was downregulated, PDP2 was induced (Fig. 1f, h). After OIS abrogation, their levels were normalized. Other PDK and PDP isozymes were not regulated in this manner (Supplementary Fig. 4c, d). Similar to cells undergoing $BRAF^{V600E}$-induced senescence, RAS^{G12V}-senescent cells showed increased accumulation of glucose-derived TCA cycle metabolites (Supplementary Fig. 5a), induction of the OCR (Supplementary Fig. 5b), a drop in PDH phosphorylation (albeit moderately, Supplementary Fig. 5c) and increased PDH enzymatic activity (Fig. 1i), but this was not accompanied by effects on PDK1 or PDP2 levels (Supplementary Fig. 5c). In quiescent cells, labelling of pyruvate, lactate, alanine and citrate from glucose-derived carbons was synchronously increased over time at a higher rate than in proliferating cells (Supplementary Fig. 6a, b), as previously reported[23]. However, the alterations in PDH activity were specific for OIS rather than a consequence of cell cycle arrest, as neither PDH phosphorylation nor PDH enzymatic activity was altered in quiescent cells (Fig. 1j, k). These results indicate that OIS, and escape thereof, is accompanied by antagonistic regulation of two key enzymes controlling PDH activity, PDP2 and PDK1.

To determine whether deregulation of the PDK1–PDP2–PDH axis drives OIS-associated metabolic rewiring, we depleted PDP2 (the expression of which is induced by $BRAF^{V600E}$). This reversed the decrease in PDH phosphorylation in OIS, leading to suppressed PDH activity (Fig. 2a, b). Consistently, [U-$^{13}C_6$]glucose and [$^{13}C_3$]pyruvate labelling revealed that PDP2-depleted cells had less labelling of citrate (Supplementary Figs 7a and 8). In agreement, the ratio of labelled [$^{13}C_2$]citrate (emulating PDH product) to [$^{13}C_3$]pyruvate (PDH substrate), indicating intracellular PDH activity, was reversed by PDP2 depletion (Fig. 2c). These cells also showed decreased OCR and redox stress compared with OIS cells (Fig. 2d and Supplementary Fig. 3b–i).

We next investigated whether PDP2 regulates OIS. Indeed, its depletion abrogated $BRAF^{V600E}$-induced arrest, which was not explained by loss of $BRAF^{V600E}$ signalling (Fig. 2a, e, f). Senescence bypass was accompanied by a marked reduction in the levels of the senescence-associated tumour suppressor $p15^{INK4B}$ (Fig. 2a) and decreased activity of the senescence-associated β-galactosidase (SA-β-gal) biomarker (Fig. 2g). Furthermore, the induction of the OIS-associated and C/EBP-β-dependent interleukins (IL)-6 and 8 (ref. 13) was curtailed by PDP2 depletion (Fig. 2h).

Because PDK1 (the expression of which is suppressed by $BRAF^{V600E}$) antagonizes PDP2 in regulating PDH activity, we also addressed its role in OIS. Ectopic restoration of PDK1 rescued the decrease in PDH phosphorylation and suppressed the increase in PDH activity in OIS cells (Fig. 3a, b). Consistently, PDK1 expression reversed the increase in TCA cycle activity in OIS cells and blocked the rise in PDH activity as judged from the [$^{13}C_2$]citrate:[$^{13}C_3$]pyruvate ratio (Fig. 3c and Supplementary Figs 7b and 8). These effects were mirrored by significant decreases in the OCR and redox stress (Fig. 3d and Supplementary Fig. 3b–i). Restoration of PDK1 expression abrogated the induction of cell cycle arrest after $BRAF^{V600E}$ expression (Fig. 3e, f), which was paralleled by suppression of several senescence-associated biomarkers (Fig. 3a, g, h). The OIS-associated metabolic rewiring was specific to the PDK1–PDP2–PDH axis: depletion of lactate dehydrogenase A

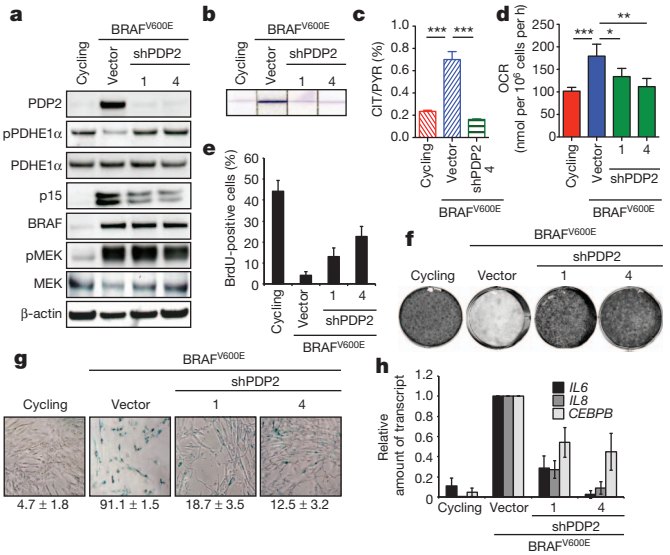

Figure 2 | PDP2 regulates metabolic rewiring and OIS. **a**, Immunoblotting analysis of HDFs expressing empty vector or shPDP2 in the presence or absence of $BRAF^{V600E}$. **b**–**g**, Cells from **a** were analysed for PDH activity in cell extracts (**b**) or intracellularly, as denoted by the [$^{13}C_2$]citrate/[$^{13}C_3$]pyruvate (CIT/PYR) ratio (**c**), the OCR (**d**), BrdU incorporation (**e**), cell proliferation (**f**) and SA-β-gal activity (**g**); $n = 3$. **h**, Regulation of *IL8*, *IL6* and *CEBPB* (also known as *C/EBP-β*) transcripts of the samples described in **a**, as determined by qRT–PCR; $n = 3$. All data are represented as mean ± s.d. $^*P < 0.05$; $^{**}P < 0.01$; $^{***}P < 0.001$.

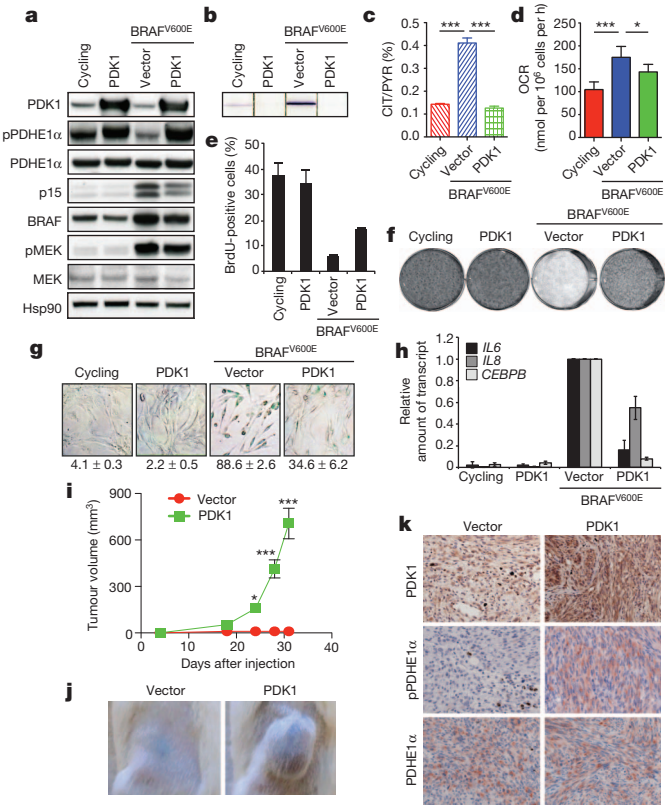

Figure 3 | PDK1 regulates metabolic rewiring and OIS, and acts tumorigenically. **a**, Immunoblotting analysis of HDFs expressing empty vector or PDK1 in the presence or absence of $BRAF^{V600E}$. **b**–**h**, Cells from **a** were analysed for PDH activity in cell extracts (**b**), or intracellularly, as denoted by the [$^{13}C_2$]citrate/[$^{13}C_3$]pyruvate ratio (**c**), the OCR (**d**), BrdU incorporation (**e**), cell proliferation (**f**), SA-β-gal activity (**g**) and *IL8*, *IL6* and *CEBPB* transcript levels (**h**); $n = 3$. **i**, Growth curve of tumours formed by p53-depleted $Braf^{V600E}$-expressing melanocytes and expressing either empty vector or PDK1; $n = 8$. **j**, **k**, Representative images (**j**) and immunohistochemical staining (original magnification, ×40) (**k**) of tumours described in **i**. Data are mean ± s.d. (**c**–**e**, **g**, **h**) or mean ± s.e.m. (**i**). $^*P < 0.05$; $^{***}P < 0.001$.

(LDHA), which stimulates mitochondrial respiration in tumour cells[24], did not change the OCR nor promote senescence, whereas $BRAF^{V600E}$ did not affect LDHA protein levels (Supplementary Fig. 9a–f). Collectively, these results show that PDP2 and PDK1 are crucially required for the metabolic wiring associated with, and the execution of, OIS.

As OIS represents a rate-limiting step in oncogenic transformation[25], we next investigated whether PDK1 can act oncogenically. Melanocytes from the skin of neonatal *Tyr::CreER; Braf*^{CA} mice[14] were depleted of *p53* (also known as *TP53*), treated with tamoxifen to induce $BRAF^{V600E}$ expression and infected with a PDK1-encoding or control virus. Whereas transplanted control melanocytes expressing *Braf*^{V600E} and short hairpin RNA (shRNA) against *p53* (shp53) failed to form tumours, ectopic expression of PDK1 induced the formation of large tumours (Fig. 3i, j and Supplementary Fig. 10a). This was associated with robust PDH phosphorylation (Fig. 3k and Supplementary Fig. 10b).

These results raised the possibility that, conversely, PDK1 depletion acts cytostatically. Indeed, its silencing from non-transformed human cells induced proliferative arrest (Fig. 4a, b and Supplementary Fig. 11a, b). This was accompanied by suppression of the DNA replication-associated protein PCNA and induction of several senescence biomarkers and tumour suppressors (Fig. 4a, c and Supplementary Fig. 11b, c), thereby underscoring the importance of PDK1 for cellular senescence. PDK1-depleted cells also showed decreased PDH phosphorylation, enhanced PDH activity and an increased OCR (Fig. 4a, d, e). Thus, PDK1 depletion from non-transformed cells, including melanocytes, causes senescence. Unexpectedly, in a panel of human BRAF mutant melanoma cell lines, this cell cycle arrest was followed by cell death a few days later (Fig. 4f and Supplementary Fig. 11d, e). This was not caused by differences in the extent of PDK1 knockdown, PDH phosphorylation or activity, nor OCR (Supplementary Figs 11f–h and 12a, b).

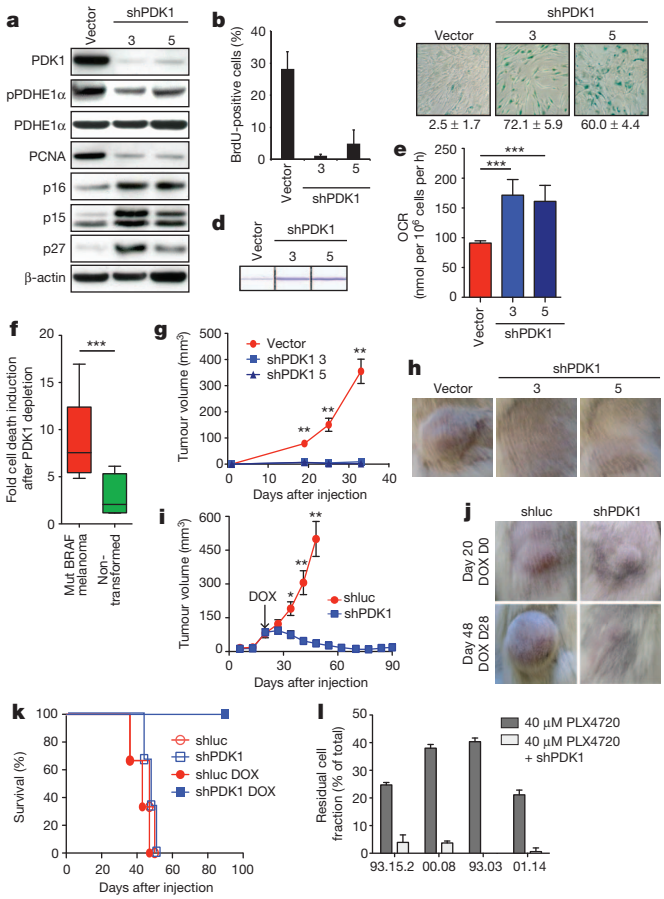

Figure 4 | PDK1 depletion causes melanoma regression and eradicates subpopulations resistant to targeted $BRAF^{V600E}$ inhibition. **a**–**e**, HDFs expressing empty vector or shPDK1 were analysed by immunoblotting (**a**) and for BrdU incorporation (**b**), SA-β-gal activity (**c**), PDH activity (**d**) and the OCR (**e**); $n = 3$. **f**, Cell death induction in melanoma ($n = 8$) and non-transformed cells ($n = 4$) after PDK1 depletion. **g**–**j**, Growth curves (**g**, **i**) and representative images (**h**, **j**) of tumours after constitutive (**g**, **h**) or DOX-inducible (**i**, **j**) PDK1 depletion; $n = 6$. **k**, Kaplan–Meier survival curve of mice from **i**. **l**, Residual cell fraction of control or PDK1-depleted melanoma cells treated with 40 μM PLX4720. Data are mean ± s.d. (**c**, **e**, **f**, **l**) or mean ± s.e.m. (**g**, **i**). $^*P < 0.05$; $^{**}P < 0.01$; $^{***}P < 0.001$.

This led to the intriguing possibility that PDK1 depletion negatively affects melanoma growth. Indeed, PDK1-depleted melanoma cell lines (which were viable at the time of inoculation) almost completely failed to produce tumours in immunocompromised mice (Fig. 4g, h and Supplementary Fig. 13a–d). A few small lesions that did develop had invariably lost PDK1 knockdown (Supplementary Fig. 13b, e), indicating that PDK1 is essential for melanoma outgrowth *in vivo*. Because, clinically, it would be more relevant to assess the role of PDK1 in tumour maintenance and progression than in initiation, we generated a doxycycline (DOX)-inducible shRNA system. DOX administration suppressed PDH phosphorylation and concomitantly caused melanoma cell death *in vitro* (Supplementary Fig. 14a–c). In mice, uninduced shPDK1 cells produced tumours indistinguishably from control cells (Supplementary Fig. 14d). By contrast, when DOX was administered starting from the time of injection, PDK1-depleted cells failed to produce tumours (Supplementary Fig. 14e). Most importantly, when DOX was administered after melanomas had established, PDK1 depletion led to near-complete tumour regression, thereby greatly extending animal survival (Fig. 4i–k). These results demonstrate that PDK1 is not only required for tumour initiation, but also for tumour maintenance and progression, indicating that it may be beneficial to target this metabolic kinase for therapeutic intervention of BRAF mutant melanoma.

Finally, we examined whether PDK1 depletion sensitizes BRAF mutant melanoma cells to treatment with PLX4720 (a preclinical analogue of vemurafenib, a specific clinical $BRAF^{V600E}$ inhibitor[26,27]). Dose–response curves of four $BRAF^{V600E}$ melanoma cell lines that are sensitive to PLX4720 (>90% cell death after treatment with 40 μM PLX4720) and another four that are partially resistant (>20% cells surviving treatment with 40 μM PLX4720) revealed that PDK1 depletion strongly sensitized all cell lines to BRAF inhibition (Supplementary Fig. 15a, b). Remarkably, PDK1 depletion specifically eliminated melanoma subpopulations that resisted high PLX4720 concentrations (Fig. 4l and Supplementary Fig. 15b). Together, these observations indicate that PDK1 depletion synergizes with targeted BRAF inhibition to kill melanoma cells.

In conclusion, by metabolic profiling and subsequent functional perturbations of a key metabolic axis, we unveil that PDH, a gatekeeper linking glycolysis to oxidative metabolism, acts as a key regulator of OIS (Supplementary Fig. 1). The observation that PDH activity is induced during OIS and normalizes after OIS abrogation highlights this enzyme as a potential barrier against malignant transformation. In agreement, high PDK1 expression drives PDH phosphorylation and promotes melanoma growth. Conversely, PDK1 depletion is highly toxic to melanoma cells. Indeed, the regression of established mutant BRAF melanomas, plus the synergistic toxicity with targeted BRAF inhibition after PDK1 depletion raise the possibility that this metabolic kinase represents an attractive combinatorial target for therapeutic intervention of BRAF mutant metastatic melanoma.

METHODS SUMMARY

The HDF cell line TIG3 expressing the ectopic receptor and human telomerase reverse transcriptase (hTERT) (or its derivative expressing $shp16^{INK4A}$), the human retinal pigment epithelial cell line RPE1, the human prostate cell line PNT1A and all BRAF mutant melanoma cell lines (A0, mel:00.08, 01.14, 04.01, 04.07, 06.04, 07.16, 93.03, 93.15.2, 634, SK-MEL-23 and SK-MEL-28) were maintained in DMEM, supplemented with 9% FBS (PAA), 2 mM glutamine, 100 U ml^{-1} penicillin and 0.1 mg ml^{-1} streptomycin (GIBCO). Melanocytes were maintained as described

previously[12]. Lentiviral and retroviral infections were performed using HEK293T cells and Phoenix cells, respectively, as producers of viral supernatants. For senescence experiments, HDFs were infected with shRNA-encoding or protein-coding retro- or lentivirus, selected pharmacologically (puromycin or blasticidin) and subsequently infected with $BRAF^{V600E}$-encoding or control virus. After selection, cells were seeded for the cell proliferation assay, BrdU incorporation assay or SA-β-gal activity, and analysed. The OCR was measured using a XF24 extracellular flux analyser (Seahorse Bioscience). Exchange rate (uptake or secretion) measurements of key metabolites and stable isotope labelling were performed as described previously[28–30]. ROS production was measured with CellROX Deep Red Reagent from Invitrogen. The GSH/GSSG ratio was determined using the GSH/GSSG-Glo assay (Promega). PDH activity was measured using the DipStick assay kit (MitoSciences). Cell death induction was measured by the trypan blue exclusion assay. Transcripts and/or protein levels of the indicated genes were determined by quantitative reverse transcription PCR (qRT–PCR) and immunoblotting or immunohistochemistry, respectively. Details are described in the Methods.

Full Methods and any associated references are available in the online version of the paper.

Received 28 February 2012; accepted 4 April 2013.
Published online 19 May 2013.

1. Campisi, J. Suppressing cancer: the importance of being senescent. *Science* **309,** 886–887 (2005).
2. Collado, M. & Serrano, M. Senescence in tumours: evidence from mice and humans. *Nature Rev. Cancer* **10,** 51–57 (2010).
3. Vredeveld, L. C. W. *et al.* Abrogation of $BRAF^{V600E}$-induced senescence by PI3K pathway activation contributes to melanomagenesis. *Genes Dev.* **26,** 1055–1069 (2012).
4. Kuilman, T., Michaloglou, C., Mooi, W. J. & Peeper, D. S. The essence of senescence. *Genes Dev.* **24,** 2463–2479 (2010).
5. Lowe, S. W., Cepero, E. & Evan, G. Intrinsic tumour suppression. *Nature* **432,** 307–315 (2004).
6. Adams, P. D. Healing and hurting: molecular mechanisms, functions, and pathologies of cellular senescence. *Mol. Cell* **36,** 2–14 (2009).
7. DeBerardinis, R. J., Sayed, N., Ditsworth, D. & Thompson, C. B. Brick by brick: metabolism and tumor cell growth. *Curr. Opin. Genet. Dev.* **18,** 54–61 (2008).
8. Tennant, D. A., Durán, R. V. & Gottlieb, E. Targeting metabolic transformation for cancer therapy. *Nature Rev. Cancer* **10,** 267–277 (2010).
9. Wellen, K. E. & Thompson, C. B. Cellular metabolic stress: considering how cells respond to nutrient excess. *Mol. Cell* **40,** 323–332 (2010).
10. Vander Heiden, M. G., Cantley, L. C. & Thompson, C. B. Understanding the Warburg effect: the metabolic requirements of cell proliferation. *Science* **324,** 1029–1033 (2009).
11. Campisi, J. Replicative senescence: an old lives' tale? *Cell* **84,** 497–500 (1996).
12. Michaloglou, C. *et al.* $BRAF^{E600}$-associated senescence-like cell cycle arrest of human naevi. *Nature* **436,** 720–724 (2005).
13. Kuilman, T. *et al.* Oncogene-induced senescence relayed by an interleukin-dependent inflammatory network. *Cell* **133,** 1019–1031 (2008).
14. Dankort, D. *et al.* $Braf^{V600E}$ cooperates with *Pten* loss to induce metastatic melanoma. *Nature Genet.* **41,** 544–552 (2009).
15. Dhomen, N. *et al.* Oncogenic Braf induces melanocyte senescence and melanoma in mice. *Cancer Cell* **15,** 294–303 (2009).
16. Davies, H. *et al.* Mutations of the *BRAF* gene in human cancer. *Nature* **417,** 949–954 (2002).
17. Wieland, O. H. The mammalian pyruvate dehydrogenase complex: structure and regulation. *Rev. Physiol. Biochem. Pharmacol.* **96,** 123–170 (1983).
18. Patel, M. S. & Roche, T. E. Molecular biology and biochemistry of pyruvate dehydrogenase complexes. *FASEB J.* **4,** 3224–3233 (1990).
19. Kolobova, E., Tuganova, A., Boulatnikov, I. & Popov, K. M. Regulation of pyruvate dehydrogenase activity through phosphorylation at multiple sites. *Biochem. J.* **358,** 69–77 (2001).
20. Roche, T. E. *et al.* Distinct regulatory properties of pyruvate dehydrogenase kinase and phosphatase isoforms. *Prog. Nucleic Acid Res. Mol. Biol.* **70,** 33–75 (2001).
21. Holness, M. J. & Sugden, M. C. Regulation of pyruvate dehydrogenase complex activity by reversible phosphorylation. *Biochem. Soc. Trans.* **31,** 1143–1151 (2003).
22. Patel, M. S. & Korotchkina, L. G. Regulation of the pyruvate dehydrogenase complex. *Biochem. Soc. Trans.* **34,** 217–222 (2006).
23. Lemons, J. M. S. *et al.* Quiescent fibroblasts exhibit high metabolic activity. *PLoS Biol.* **8,** e1000514 (2010).
24. Fantin, V. R., St-Pierre, J. & Leder, P. Attenuation of LDH-A expression uncovers a link between glycolysis, mitochondrial physiology, and tumor maintenance. *Cancer Cell* **9,** 425–434 (2006).
25. Mooi, W. J. & Peeper, D. S. Oncogene-induced cell senescence–halting on the road to cancer. *N. Engl. J. Med.* **355,** 1037–1046 (2006).
26. Tsai, J. *et al.* Discovery of a selective inhibitor of oncogenic B-Raf kinase with potent antimelanoma activity. *Proc. Natl Acad. Sci. USA* **105,** 3041–3046 (2008).
27. Flaherty, K. T., Yasothan, U. & Kirkpatrick, P. Vemurafenib. *Nature Rev. Drug Discov.* **10,** 811–812 (2011).
28. Frezza, C. *et al.* Haem oxygenase is synthetically lethal with the tumour suppressor fumarate hydratase. *Nature* **477,** 225–228 (2011).
29. Frezza, C. *et al.* Metabolic profiling of hypoxic cells revealed a catabolic signature required for cell survival. *PLoS ONE* **6,** e24411 (2011).
30. Chaneton, B. *et al.* Serine is a natural ligand and allosteric activator of pyruvate kinase M2. *Nature* **491,** 458–462 (2012).

Supplementary Information is available in the online version of the paper.

Acknowledgements We thank J.-Y. Song for pathological analysis, M. McMahon for providing $Braf^{CA}$ mice, C. Vogel for sharing cell lines, R. van Amerongen for critical reading of the manuscript, and all members of the Gottlieb and Peeper laboratories for their input. This work was supported by Cancer Research UK, Spanish Government-EU-FEDER (grants SAF2011-25726 and ISCIII-RTICC-RD6/0020/0046) and ICREA-Academia to M.C., Israel Cancer Research Foundation and Israel Science Foundation to T.S., a Vici grant from the Netherlands Organization for Scientific Research (NWO) and a Queen Wilhelmina Award grant from the Dutch Cancer Society (KWF Kankerbestrijding) to D.S.P.

Author Contributions J.K., E.G. and D.S.P. conceived the project, analysed the data and wrote the manuscript. J.K. performed all *in vitro* experiments and carried out the *in vivo* experiments together with K.M. J.K., K.M. and B.C. performed metabolic experiments. L.Z. and G.M. performed LC–MS analyses. S.H.B. and E.M.E.V. provided low passage melanoma cell lines. V.A.S., M.C. and T.S. helped with metabolic analyses. All authors discussed the results and commented on the manuscript. E.G. and D.S.P. contributed equally to this work.

Author Information Reprints and permissions information is available at www.nature.com/reprints. The authors declare competing financial interests: details are available in the online version of the paper. Readers are welcome to comment on the online version of the paper. Correspondence and requests for materials should be addressed to E.G. (e.gottlieb@beatson.gla.ac.uk) or D.S.P. (d.peeper@nki.nl).

METHODS

Cell culture, viral transduction and senescence induction. The HDF cell line TIG3 expressing the ectopic receptor and human telomerase reverse transcriptase (hTERT) (or its derivative expressing shp16^{INK4A}), the human retinal pigment epithelial cell line RPE1, the human prostate cell line PNT1A and all BRAF mutant melanoma cell lines (A0, mel:00.08, 01.14, 04.01, 04.07, 06.04, 07.16, 93.03, 93.15.2, 634, SK-MEL-23 and SK-MEL-28) were maintained in DMEM, supplemented with 9% FBS (PAA), 2 mM glutamine, 100 U ml^{-1} penicillin and 0.1 mg ml^{-1} streptomycin (GIBCO). Melanocytes were maintained as described previously[12]. Lentiviral and retroviral infections were performed using HEK293T cells and Phoenix cells, respectively, as producers of viral supernatants. For senescence experiments, HDFs were infected with shRNA-encoding or protein-coding retro- or lentivirus, selected pharmacologically (puromycin or blasticidin) and subsequently infected with BRAF^{V600E}-encoding or control virus. After selection, cells were seeded for the cell proliferation assay, BrdU incorporation assay or SA-β-gal activity, and analysed.

Measurement of metabolites by LC–MS. Stable isotope labelling was performed as described previously[28]. Two-million HDFs were plated onto 10-cm dishes and cultured in standard medium for 24 h. For stable isotope labelling analysis, the medium was replaced with 4.5 mM [U-^{13}C]glucose (Cambridge Isotope). After incubation for the indicated time, cells and media were collected. For extracellular metabolite analysis, 200 µl of growth medium from cell culture were added to 600 µl of acetonitrile for deproteinization. Samples were vortexed for 10 min and centrifuged for 10 min at 16,000*g* at 4 °C. The supernatant was stored for subsequent liquid chromatograph–mass spectrometry (LC–MS) analysis. For intracellular metabolite analysis, cells were lysed with a solution consisting of 50% methanol and 30% acetonitrile in water in dry ice methanol (−80 °C) and quickly scraped from the plate. The insoluble material was immediately pelleted in a cooled centrifuge (4 °C) for 10 min at 16,000*g*, and the supernatant was collected for subsequent LC–MS analysis. For [U-^{13}C]pyruvate labelling analysis, samples were processed as for the ^{13}C-labelled glucose labelling analysis, except that the medium was not replaced, but spiked with 0.11 mg ml^{-1} [$^{13}C_3$]sodium pyruvate (Cambridge Isotope). LC–MS analysis was carried out as described previously[29]. Mass spectrometry data were analysed by LCquan (Thermo Scientific), and quantifications of intracellular and extracellular metabolites were performed by the standard dilution method as described previously[30].

Cell proliferation assay. Cells were seeded into a six-well plate (at densities of 2×10^5, 4×10^5 or 6×10^5 cells) and selected pharmacologically. Fixation and staining with crystal violet was performed 9–13 days after the BRAF^{V600E}-encoding or control virus infection, or 6–9 days after shPDK1-encoding or control virus infection. Images of cell proliferation assays reflect representative results of at least three independent experiments.

BrdU incorporation assay. BrdU labelling was carried out for 3 h followed by fixation. Incorporated BrdU was detected by immunostaining as described previously[31] and by FACS analysis. Results are represented as mean and s.d. of at least three independent experiments.

Analysis of SA-β-gal activity. SA-β-gal was stained using the Senescence Associated β-Galactosidase Staining kit (Cell Signaling) at pH 6, according to the manufacturer's protocol. Images reflect representative results of at least three independent experiments.

Trypan blue exclusion assay. Cells were brought into suspension using trypsin, centrifuged and resuspended in a small volume of culture medium. Trypan blue (Sigma) was added to the cell suspension (dilution factor = 2) and stained cells were counted as dead. The number of dead cells was quantified, and the values were expressed as the fold change over control. Results are represented as mean and s.d. of at least three independent experiments.

Measurement of redox stress. ROS production was measured with CellROX Deep Red Reagent from Invitrogen. Cells were incubated at 37 °C for 30 min in DMEM supplemented with 9% FBS (PAA) and containing 2.5 µM CellROX Deep Red Reagent. Cells were then washed twice in PBS, treated with trypsin and resuspended in PBS supplemented with 50% FCS. Fluorescence was immediately measured using FACS analysis.

The GSH/GSSG ratio was determined using the GSH/GSSG-Glo assay (Promega) according to the manufacturer's protocol. Results are represented as mean and s.d. of at least three independent experiments.

Plasmids. pMSCV-blast-BRAF^{V600E} and pMSCV-blast were previously described[13]. For the overexpression of PDK1, *PDK1* derived from complementary DNA of a normal human skin sample was PCR-amplified and cloned into pLZRS-IRES-puro or FG12-eGFP. Empty pLZRS-IRES-puro or FG12-eGFP was used as a control.

shRNAs. Retroviral knockdown constructs were described previously[12,13]. Lentiviral constitutive knockdown constructs were purchased from Sigma-Aldrich in pLKO.1 backbone or cloned (shp53) into KH1eGFP backbone (a gift from M. Soengas): shPDP2-1 (clone TRCN0000036739), 5′-CCTTGAAAGCAGAGTCCCAAA-3′; shPDP2-4 (TRCN0000036742) 5′-GCTGAAGTGGAGTAAAGAGTT-3′; shPDK1-3 (TRCN0000006261) 5′-GCTCTGTCAACAGACTCAATA-3′; shPDK1-5 (TRCN0000006263) 5′-CCAGGGTGTGATTGAATACAA-3′; shp53 mouse, 5′- GTACATGTGTAATAG CTCC-3′.

As negative controls pRS-puro, pLKO.1-puro or KH1eGFP without insert were used. Lentiviral-inducible knockdown plasmid pLKO.1-Tet-On was purchased from Addgene. shRNA targeting PDK1 were re-cloned from the constitutive shPDK1-3 knockdown construct. As negative control pLKO.1-Tet-On with shRNA targeting luciferase was used: shluc, 5′-CGCTGAGTACTTCGAAATGTC-3′.

qRT–PCR. Total RNA was DNase-treated with RQ1 RNase-Free DNase (Promega). Reverse transcription was performed with SuperScript II First Strand Kit (Invitrogen). qRT–PCR was performed with the SYBR Green PCR Master Mix (Applied Biosystems) on an ABI PRISM 7700 Sequence detection system.

IL6, *IL8*, *CEBPB* and *RPL13* (standard) primer sequence were described previously[13]. Other primer sets used were as follows: *PDK1*, 5′-CCAAGACCTCGTGTTGAGA CC-3′ and 5′-AATACAGCTTCAGGTCTCCTTGG-3′; *PDK2*, 5′-GAGCCTCC TGGACATCATGG-3′ and 5′-TACTCAAGCACGCCTTGTGC-3′; *PDK3*, 5′-A CTGTATTCCATGGAAGGAGTGG-3′ and 5′-CTCCAATCATCGGCTTCAG G-3′; *PDK4*, 5′-AACTGTGATGTGGTAGCAGTGG-3′ and 5′-GATGTGAATT GGTTGGTCTGG-3′; *PDP2*, 5′-ACCACCTCCGTGTCTATTGG-3′ and 5′-CC AGCGAGATGTCAGAATCC-3′; *NQO1*, 5′-CAGCTCACCGAGAGCCTAGT-3′ and 5′-GAGTGAGCCAGTACGATCAGTG-3′; *GCLC*, 5′-ATGCCATGGGA TTTGGAAT-3′ and 5′-AGATATACTGCAGGCTTGGAATG-3′; *GSTA4*, 5′-AG TTGTACAAGTTGCAGGATGG-3′ and 5′-CAATTTCAACCATGGGCACT-3′; *GSTM4*, 5′-TCATCTCCCGCTTTGAGG-3′ and 5′-CAGACAGCCACCCTTGT GTA-3′; *HMOX1*, 5′-GGGTGATAGAAGAGGCCAAGA-3′ and 5′-AGCTCCTG CAACTCCTCAAA-3′; *SOD1*, 5′-TCATCAATTTCGAGCAGAAGG-3′ and 5′-CA GGCCTTCAGTCAGTCCTTT-3′; *SOD2*, 5′-CTGGACAAACCTCAGCCCTA-3′ and 5′-TGATGGCTTCCAGCAACTC-3′.

Except for *CEBPB*, all primer pairs span exon–exon borders. *RPL13* was used as a control. For analysis, the ΔC_T method was applied. Data are represented as mean ± s.d. of three or more independent experiments.

Antibodies. Antibodies used for immunoblotting/immunohistochemistry were β-actin (AC-74; A5316; Sigma), BRAF (sc-5284; Santa Cruz), Hsp90 (4874; Cell Signaling), LDHA (2012; Cell Signaling), MEK1/2 (L38C12; 4694; Cell Signaling), phospho-MEK1/2 (Ser 217/221) ((41G9); 9154; Cell Signaling), PCNA ((PC10); sc-56; Santa Cruz), PDHE1α ((9H9AF5); 459400; Invitrogen), phospho-PDHE1α (Ser 293) (AP1062; Calbiochem), PDK1 (KAP-PK112; Stressgene), PDP2 (HPA01995; Sigma), p16^{INK4A} ((JC3); sc-56330; Santa Cruz), p27^{Kip1} (610241; BD Transduction Laboratories), and p15^{INK4B} (sc-612; Santa Cruz).

Immunohistochemistry. Formalin-fixed paraffin-embedded tissue samples were stained according to common procedures. For antigen retrieval, samples were incubated in 20 µg ml^{-1} proteinase K (Z0622, Sigma for PDK1), in citrate buffer (Biogenex, for PDHE1α) or in Tris-EDTA, pH 9.0 (for phosphor-PDHE1α (Ser 293)). Sections were counterstained with haematoxylin.

Drug treatment. For dose–response curves, melanoma cells were treated with the indicated concentrations of PLX4720 (Selleck) for 3 days. Cell viability was determined with the Cell Titer Blue assay (Promega) and fluorescence was measured with a TECAN infinite scanner. Results represent at least three independent experiments.

***In vivo* assays.** All mouse experiments were performed according to a protocol approved by the Institutional Animal Experiment Ethics Committee. Experiments were repeated at least twice.

Murine melanocyte derivation, culture and tumour growth *in vivo*. Melanoytes were derived from neonatal skin of *Tyr::CreER;Braf^{CA}* mice[14], as described previously[32]. Primary melanocyte cultures were prepared on a mitomycin-treated XB2 (immortal murine keratinocytes) feeder cell layer for one passage only. Cells were grown in RPMI medium supplemented with 5% FCS, 200 nM 12-*O*-tetradecanoyl phorbol 13-acetate, 200 pM cholera toxin, 10 ng ml^{-1} recombinant stem cell factor (SCF; R&D Systems) and 100 nM endothelin 3 (Bachem) at 37 °C and under low oxygen conditions (5% CO_2 and 3% O_2). Primary melanocytes were transduced with retro- or lentivirus in the presence of 2 µg ml^{-1} polybrene overnight. The transduction with lentivirus delivering shRNA targeting p53 and the PDK1 expression vector were done on consecutive nights. The transduction of virus allowing PDK1 expression was repeated two to four times. In addition, melanocytes were treated with 0.2 µM 4-hydroxytamoxifen for at least 9 days to induce the expression of BRAF^{V600E} by switching from the conditional to the mutated allele. One week after the last transduction, 1×10^6–1.5×10^6 melanocytes (dependent on the experiment) were subcutaneously injected with 50% basement membrane Matrigel (growth factors reduced) into both flanks of NSG mice (NOD *scid* IL2 receptor gamma chain knockout mice). Tumour volume was determined by measurement of two dimensions and calculation with the following formula: $V = 4/3 * \pi * a^2 * b$, in which a is the shorter and b is the longer dimension. BRAF allele rearrangements

in tumours were detected by PCR as previously described[33]. Tumours were analysed by immunohistochemistry and immunoblot.

Xenograft experiments. NOD/*scid* mice were subcutaneously injected with 0.5×10^6 cells into both flanks. For DOX-inducible shRNA xenograft experiments, mice were exposed to 2 mg ml^{-1} DOX administered in 5% sucrose-containing drinking water, either directly after injection or when tumours reached a volume of 100 mm^3. Mice were inspected twice a week and euthanized by CO_2 when tumours reached the volume of 500 mm^3 (1,000 mm^3 per mouse). Tumour volume was determined as above.

Measurement of OCR. Basal OCR was measured using the XF24 extracellular flux analyser (Seahorse Bioscience). At the end of the experiment, 1 mmol l^{-1} antimycin A was added to measure mitochondria-independent oxygen consumption. Each cycle of measurement consisted of 3 min mixing, 3 min waiting and 4 min measuring. OCR was normalized to the cell number calculated at the end of the experiments. To obtain the mitochondrial-dependent OCR, only the antimycin-sensitive respiration was used. Homogeneous plating of the cells and cell count were assessed by fixing the cells with trichloroacetic acid 10% for 1 h at 4 °C and then staining the fixed cells with a 0.47% solution of sulphorhodamine B (Sigma).

Measurement of PDH activity. PDH activity in cell lysates was measured using the DipStick assay kit from MitoSciences (MSP90). Cells were lysed in the sample buffer provided by the manufacturer, followed by centrifugation and measurement of the protein concentration with the BioRad Protein Assay. One-hundred-and-forty milligrams of protein lysate was loaded and PDH activity was measured according to the manufacturer's protocol.

Statistical analysis. Statistical analyses of metabolite exchange rates were done with *t*-tests. Analysis of all other data was done with a non-parametric two-tailed Mann–Whitney *U* test with a 95% confidence interval (Prism; GraphPad Software). $P < 0.05$ was considered significant.

31. Serrano, M., Lin, A. W., McCurrach, M. E., Beach, D. & Lowe, S. W. Oncogenic *ras* provokes premature cell senescence associated with accumulation of p53 and $p16^{INK4a}$. *Cell* **88,** 593–602 (1997).
32. Sviderskaya, E. V. *et al.* Complementation of hypopigmentation in *p*-mutant (*pink-eyed dilution*) mouse melanocytes by normal human P cDNA, and defective complementation by OCA2 mutant sequences. *J. Invest. Dermatol.* **108,** 30–34 (1997).
33. Dankort, D. *et al.* A new mouse model to explore the initiation, progression, and therapy of $BRAF^{V600E}$-induced lung tumors. *Genes Dev.* **21,** 379–384 (2007).